Simplified and Detailed Analysis of Data Center Particulate Contamination at Server and Room Level Using Computational Fluid Dynamics

Satyam Saini[1]
Mechanical and Aerospace Engineering Department,
The University of Texas at Arlington,
Arlington, TX 76019
e-mail: satyam.saini@mavs.uta.edu

Pardeep Shahi
Mechanical and Aerospace Engineering Department,
The University of Texas at Arlington,
Arlington, TX 76019

Pratik Bansode
Mechanical and Aerospace Engineering Department,
The University of Texas at Arlington,
Arlington, TX 76019

Jimil M. Shah
Mechanical and Aerospace Engineering Department,
The University of Texas at Arlington,
Arlington, TX 76019

Dereje Agonafer
Mechanical and Aerospace Engineering Department,
The University of Texas at Arlington,
Arlington, TX 76019

Continuous rise in cloud computing and other web-based services propelled the data center proliferation seen over the past decade. Traditional data centers use vapor-compression-based cooling units that not only reduce energy efficiency but also increase operational and initial investment costs due to involved redundancies. Free air cooling and airside economization can substantially reduce the information technology equipment (ITE) cooling power consumption, which accounts for approximately 40% of energy consumption for a typical air-cooled data center. However, this cooling approach entails an inherent risk of exposing the ITE to harmful ultrafine particulate contaminants, thus, potentially reducing the equipment and component reliability. The present investigation attempts to quantify the effects of particulate contamination inside the data center equipment and ITE room using computational fluid dynamics (CFD). An analysis of the boundary conditions to be used was done by detailed modeling of ITE and the data center white space. Both two-dimensional and three-dimensional simulations were done for detailed analysis of particle transport within the server enclosure. An analysis of the effect of the primary pressure loss obstructions like heat sinks and dual inline memory modules inside the server was done to visualize the localized particle concentrations within the server. A room-level simulation was then conducted to identify the most vulnerable locations of particle concentration within the data center space. The results show that parameters such as higher velocities, heat sink cutouts, and higher aspect ratio features within the server tend to increase the particle concentration inside the servers. [DOI: 10.1115/1.4053363]

[1]Corresponding author.

Contributed by the Electronic and Photonic Packaging Division of ASME for publication in the Journal of Electronic Packaging. Manuscript received March 31, 2021; final manuscript received December 20, 2021; published online January 28, 2022. Assoc. Editor: Jaeho Lee.

1 Introduction

Data center energy consumption continues to rise with increasing computational, storage, and networking demands due to developments in Artificial Intelligence and machine learning, bitcoin mining, and cloud computing. While cooling technologies like dielectric fluid immersion cooling (single-phase and two-phase) [1–3] and direct-to-chip liquid cooling using cold plates [4,5] are being used to dissipate significantly high heat fluxes, air cooling still dominates the data center cooling industry, and it might continue as such.

Conventional air-cooled data centers operate year-round using mechanical cooling without taking the advantage of seasonal or local climatic conditions to cool the information technology equipment (ITE). Airside economization or free air cooling can accomplish this by bringing outside air at low ambient temperature and relative humidity to reduce the compressor work partly or completely for a major part of the year, thus, saving energy expenditure. The ASHRAE T.C.9.9 subcommittee on Mission Critical Facilities, Data Centers, Technology Spaces, and Electronic equipment expanded the recommended thermal and humidity envelopes, thereby, allowing short excursions into the allowable regions A1–A4, as shown in Fig. 1, and an increase in the number of economizer hours. While companies like Microsoft and Facebook have been able to achieve power usage effectiveness values as low as 1.1 using free air-cooling methods in geographies with favorable climatic conditions throughout the year, many data center administrators are still reluctant to implement airside economization [6–9]. This is owed to the inherent risk of introducing fine particulate and corrosive gaseous contaminants along with the outside air. For data centers using airside economization for cooling, ASHRAE recommends a minimum efficiency reporting value (MERV) 11–13 filters for outside air filtration and MERV 8 filters for continuously filtering data center indoor air [10]. A summary of the contaminant arresting efficiency of various MERV filters is shown in Fig. 2.

The issue being investigated in this study is utilizing tools like computational fluid dynamics (CFD) for data center particle flow visualization and addressing the lack of studies that specifically look into issue data center contamination. It is extremely difficult to otherwise, conduct tightly controlled experiments with particle visualization and particle generating equipment, where the cost can reach hundreds of thousands of dollars for the state-of-the-art equipment. The authors, therefore, propose using CFD tools that use well-established particle and flow interaction correlations to simulate the contaminant flow in data center flow boundary conditions. The challenging part of simulating particle flow inside the servers and data center is the presence of a multitude of bluff bodies of varying geometries that produce eddies that produce numerous adverse pressure gradients around these objects. Based on an extensive literature review, it was identified that a knowledge gap exists in terms of an approach to identify discrete locations of particle accumulation inside the ITE and at the data center level. The issue of data center contamination due to settled particulate matter has been mostly discussed in the form of case studies, from a risk assessment point of view, and mostly addresses the best practices to mitigate harmful contaminants [11,12]. The current literature is dominated by empirical studies that have investigated the failure modes and failure mechanisms, dominated by corrosion studies at printed circuit board level and interconnect level. Particle-laden flow, in general, has been studied widely for commercial buildings and indoor residential environments owing to the high risk to the occupants [13–15].

The results investigated in this study are divided into two main sections: particle flow patterns at the ITE level and particle flow pattern analysis at room level. This study is an extension of the authors' previously published work where a simplified model of a raised floor data center space was developed to visualize particle transport at room level [16]. A similar approach was used in this study, where a transient CFD analysis was done for simplified two-dimensional (2D) and three-dimensional (3D) models of the

Class[a]	Equipment Environmental Specifications for Air Cooling						
	Product Operations[b,c]					Product Power Off[c,d]	
	Dry-Bulb Temperature[e,g] °C	Humidity Range, Non-Condensing[h,i,k,l]	Maximum Dew Point[k] °C	Maximum Elevation[e,j,m] m	Maximum Temperature Change[f] in an Hour (°C)	Dry-Bulb Temperature °C	Relative Humidity[k] %
Recommended (Suitable for all 4 classes)							
A1 to A4	18 to 27	-9°C DP to 15°C DP and 60% RH					
Allowable							
A1	15 to 32	-12°C DP & 8% RH to 17°C DP and 80% RH[k]	17	3050	5/20	5 to 45	8 to 80
A2	10 to 35	-12°C DP & 8% RH to 21°C DP and 80% RH[k]	21	3050	5/20	5 to 45	8 to 80
A3	5 to 40	-12°C DP & 8% RH to 24°C DP and 85% RH[k]	24	3050	5/20	5 to 45	8 to 80
A4	5 to 45	-12°C DP & 8% RH to 24°C DP and 90% RH[k]	24	3050	5/20	5 to 45	8 to 80
B	5 to 35	8% to 28°C DP and 80% RH[k]	28	3050	NA	5 to 45	8 to 80
C	5 to 40	8% to 28°C DP and 80% RH[k]	28	3050	NA	5 to 45	8 to 80

Fig. 1 ASHRAE 2015 temperature guidelines showing the recommended and allowable ranges for temperature and humidity for data centers

servers with large obstructions like heat sinks, dual inline memory modules (DIMMs) were created for different server configurations. The flow and particle transport models were studied from existing literature on particle transport in ducts and 2D channels and 3D ducts with and without obstructions. This enabled the authors to significantly simplify the problem and formulate a set of assumptions that closely matched the flow characteristics inside a real server. The particle dispersion results were reported by analyzing the time spent by a specified particle mass flow rate in the flow domain, the particle mass entering and leaving the domain at a steady-state, and the average instantaneous particle volume fraction in the domain. Further analysis was also done to identify and compare various geometries and heat sink configurations from a thermal point of view to ascertain the tradeoffs in thermal performance and particle accumulation.

2 Numerical Method

Particle-laden flow is a common phenomenon for many practical daily indoor and technical applications. CFD enables detailed prediction of complex fluid flows by discretizing complex geometries into smaller regions and numerically solving the desired flow characteristics in these individual discretized regions. Commercially available CFD codes have made it easier to visualize complicated flow phenomena like particle–particle interactions and particle-flow interactions. The Lagrange–Euler approach has been proven to solve multiphase particle-laden flows. This approach uses Reynolds-averaged Navier–Stokes (RANS) equations to solve the continuous or carrier phase and the dispersed or particle phase is resolved by Lagrangian tracking. The CFD code was chosen based on its extensive abilities in resolving particle–particle, particle–flow interactions, and accurate mathematical models in simulating turbulence involved in particle flow. As described in ANSYS FLUENT theory guide [17,18], the continuous phase is calculated using the RANS equations as given below:

$$\nabla.\overline{u} = 0 \tag{1}$$

$$\frac{\partial u}{\partial t} + \rho\,(\overline{u}.\nabla)\overline{u} = -\nabla\overline{p} + \eta\Delta\overline{u} - \nabla.\overline{\tau^{RS}} + \overline{f}_D \tag{2}$$

where $\overline{u}$ and $\overline{p}$ are the average velocities of continuous (air) and discrete (particle) phases. The second term on the left-hand side in Eq. (2) represents the Reynolds stresses which are modeled using the eddy-viscosity approach. In this study, the standard κ–ω model was used to model kinetic energy and turbulent dissipation. Equations (3)–(5) are solved to obtain the particle force balance and particle trajectories of particles of mass m_p

$$m_p\frac{d\mathbf{u_p}}{dt} = \sum\overline{F_i} \tag{3}$$

$$\sum\overline{F_i} = \overline{F_D} + \overline{F_B} + \overline{F_G} \tag{4}$$

$$m_p\frac{d\mathbf{u_p}}{dt} = m_p\frac{\mathbf{u}-\mathbf{u}_p}{\tau_r} + m_p\frac{\mathbf{u}(\rho_p-\rho)}{\rho_p} + \mathbf{F} \tag{5}$$

3 Methodology

To generalize the CFD results of particle dispersion, a set of assumptions was formulated that would most closely match flow parameters and conditions in a typical air-cooled data center. The overall simulation setup including the inputs required for particle-phase, turbulence model used, and type of boundary conditions applied, stays the same for 2D, 3D as well as room-level simulations. The range of particle diameter considered in this study is between 10 μm and 0.01 μm with a mean diameter of 5 μm. A total of 15 different diameters were generated between this range to judge the dispersion of well-distributed particle sizes in the flow domain. Various cases that have been simulated are tabulated in Table 1 and an example of simplified 2D geometries analyzed is shown in Fig. 3. These cases were simulated with two-particle densities and two different flow velocities. The particle densities chosen were 1550 kg/m^3 and 4000 kg/m^3, and the velocities were chosen to be 0.8 m/sec and 2.5 m/sec. The densities and were chosen based on data from literature of most pervasive and corrosive ionic salts and particulate matter [19]. The cases with multiple geometries were sliced to form sweepable faces for a structured grid. The maximum mesh count among all the 2D cases was 439,000 which is significantly lower than that obtained in the 3D model case. For 3D simulations, using similar meshing operations, the maximum grid count of 2.6×10^6 was obtained.

MERV RATING CHART

Standard 52.5 Minimum Efficiency Reporting Value	Dust Spot Efficiency	Arrestance	Typical Controlled Contaminant	Typical Applications and Limitations	Typical Air Filter/Cleaner Type
20	n/a	n/a	< 0.30 pm particle size	Cleanrooms	>99.999% eff. On .10-.20 pm Particles
19	n/a	n/a	Virus (unattached)	Radioactive Materials	Particles
18	n/a	n/a	Carbon Dust	Pharmaceutical Man.	Particulates
17	n/a	n/a	All Combustion smoke	Carcinogenetic Materials	>99.97% eff. On .30 pm Particles
16	n/a	n/a	.30-1.0 pm Particle Size	General Surgery	**Bag Filter**- Nonsupported
15	>95%	n/a	All Bacteria	Hospital Inpatient Care	microfine fiberglass or
14	90-95%	>98%	Most Tobacco Smoke	Smoking Lounges	synthetic media, 12-36 in. deep, 6-12 pockets
					Box Filter- Rigid Style Cartridge Filters 6 to 12" deep m ay use
13	89-90%	>98%	Proplet Nuceli (Sneeze)	Superior Commercial Buildings	lofted or paper media.
12	70-75%	>95%	1.0-3.0 pm Particle Size	Superior Residential	**Bag Filter**- Nonsupported
			Legionella		microfine fiberglass or
11	60-65%	>95%	Humidifier Dust	Better Commercial Buildings	synthetic media, 12-36 in. deep, 6-12 pockets
			Lead Dust		
					Box Filter- Rigid Style Cartridge Filters 6 to 12" deep m ay use lofted or paper media.
10	50-55%	>95%	Milled Flour		
			Auto Emissions	Hospital Laboratories	
9	40-45%	>90%	Welding Fumes		
8	30-35%	>90%	3.0-10.0 pm Particle Size	Commercial Buildings	**Pleated Filters**- Disposable, extended surface area, thick with cotton-polyester blend media, cardboard frame
			Mold Spores		
7	25-30%	>90%	Hair Spray	Better Residential	**Cartridge Filters**- Graded density viscous coated cube or pocket filters, synthetic media
			Fabric Protector		
6	<20%	85-90%	Dusting Aids	Industrial Workplace	**Throwaway**- Disposable synthetic panel filter.
			Cement Dust		
5	<20%	80-85%	Pudding Mix	Paint Booth Inlet	
4	<20%	75-80%	>10.0 pm Particle Size	Minimal Filtration	**Throwaway**- Disposable fiberglass or synthetic panel filter.
			Pollen		
3	<20%	70-75%	Dust Mites	Residential	**Washable**- Aluminum Mesh
			Sanding Dust		
2	<20%	65-70%	Spray Paint Dust		
					Electrostatic- Self charging woven panel filter.
			Textile Fibers	Window A/C Units	
1	<20%	<65%	Carpet Fibers		

Fig. 2 Summary of different MERV filter efficiency and their particle arrestance efficiency at varying particle diameters

Table 1 Description of simulated cases

S. no.	Case type
1	Two heat sinks inline
2	Two heat sinks side by side
3	Heat sink with round edge
4	Heat sink with sharp edges
5	Blade server
6	Staggered heat sink arrangement
7	Heat sink with cutout

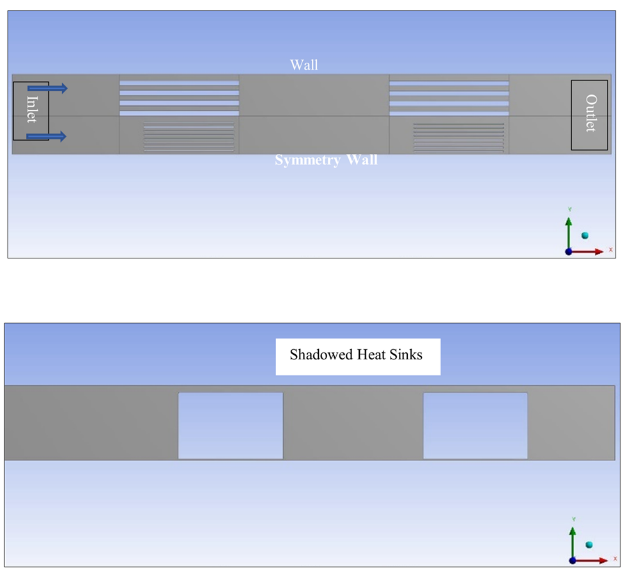

Fig. 3 Examples of the simplified 2D geometries of servers and boundary conditions used for simulations showing (*a*) heat sink and DIMMs and (*b*) heat sinks in line from the side view

4 Results and Discussion

The results presented in this section are divided into results from 2D simulations, results obtained from 3D simulations, and results for room-level simulations. The results obtained from 2D simulations were also compared with 3D simulations to quantify the discrepancy between the results. To resolve the near-wall boundary layers at higher velocities, inflation layers were used as shown in Fig. 4.

4.1 Two-Dimensional Results for Information Technology Equipment

4.1.1 Sharp-Edged Heat Sink Versus Curve Edged. A lot of heat sinks are manufactured with curved edges, especially for

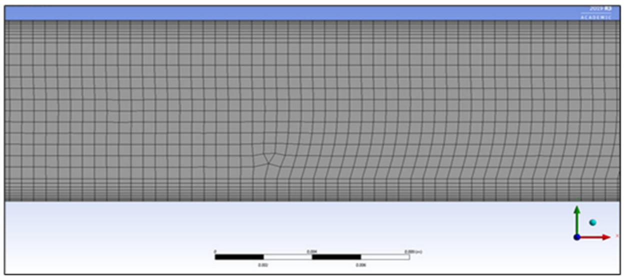

Fig. 4 Inflation layers created at the walls to capture near-wall velocity gradients and particle concentrations

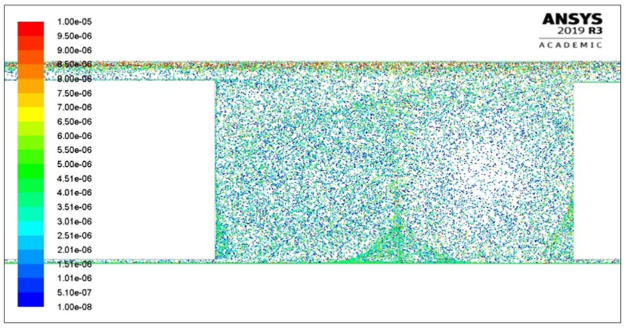

(*a*)

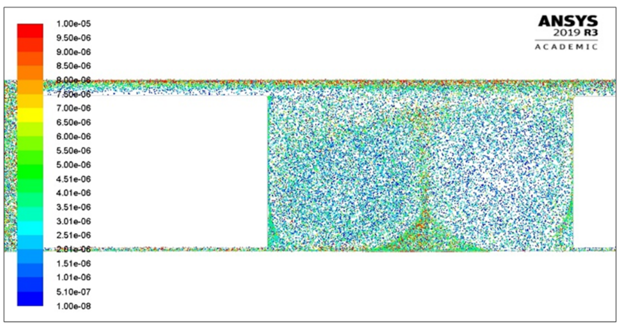

(*b*)

Fig. 5 Particle diameters in the flow domain for dispersion from (*a*) sharp and (*b*) round-edged heat sinks

servers requiring very high airflow rates, to reduce the overall pressure drop in the system. This decelerates the flow at the corners, keeping the turbulent mixing between the fins for effective heat removal. In this case, 2D geometries were designed with dimensions equivalent to that of a 2 U server and a heat sink height of 7.8 cm. As seen in Figs. 5(*a*) and 5(*b*), for sharp-edged heat sink, more particle diameters were present on the heat sink in sharp edge than in the case of the round edge heat sink. Also, as opposed to that, more particle diameters were present between heat sinks in case round-cornered than sharp edge heat sink Furthermore, a greater number of the particles moved toward the top of the server for the round edge heat sink. A comparison of particle flow parameters is given in Table 2. It can be concluded that more particles stay in the flow domain for sharp-cornered heat sinks. This can be attributed to the fact that sharp edges tend to shed more vortices, trapping the particles of larger diameters around them due to the centrifugal forces. This has also been reported in the published literature.

4.1.2 Heat Sink Side by Side Versus in-Line. As seen in Figs. 6(*a*) and 6(*b*), high particle residence time was obtained at the walls of in-line heat sinks toward the rear end of the server. Other locations of relatively higher residence time were between the heat sink and the DIMMs. Another inference that can be made

Table 2 Particle summary for the sharp edge and curved edge heat sink

Sharp edge	
Parameter	Value
Total mass injected	5×10^{-20} kg
Escaped outlet	3.9×10^{-16} kg
Max time in domain	2.36×10^{-1} sec
Min time in the domain	4.93 sec
Curved edge	
Parameter	Value
Total mass injected	5×10^{-20} kg
Escaped outlet	4.5×10^{-20} kg
Min time in the domain	2.30×10^{-1} sec
Max time in the domain	4.64 sec

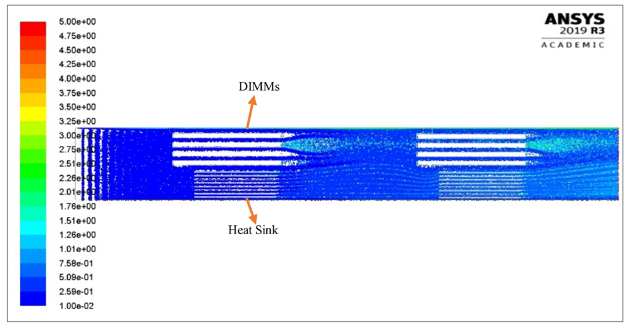

(*a*)

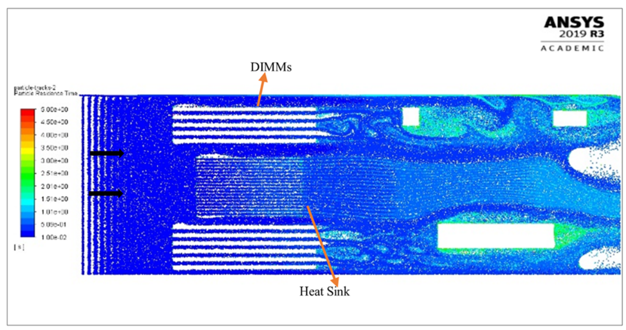

(*b*)

Fig. 6 Particle residence time in the flow domain for (*a*) in-line heat sinks and (*b*) side by side heat sinks

from Fig. 6(*b*) is that solid obstructions behind the heat sinks with greater depth do not create large turbulent eddies or any vortex shedding when compared to square or circular obstructions. It can thus be pointed out that there might be a greater probability of finding settled particulate matter toward the rear end of the servers of similar geometries. These regions mostly contain drive backplanes, power supplies, drive fillers, etc. Table 3 shows the comparison particle summary for both the cases discussed in this section. Here, it can be noted that for both cases, the maximum time spent by the particles in the flow domain was identical, but the average time was more in the case of heat sinks located side by side.

4.1.3 Effect of Velocity. Figures 7(*a*) and 7(*b*) show the impact of increasing inlet velocity on particle accumulation, two different values of velocities were chosen from published literature [20]. The particle residence time plots depict that for lower velocity values, particles spend more time in the flow domain and for high velocity, particles spend more time on the surfaces. This phenomenon holds when compared to the conclusions made by Frankenthal et al. [21]. No deposition on the top or bottom wall for high velocity was observed until the flow reaches the second

Table 3 Particle summary for heat sinks arranged side by side high density and inline

Inline heat sinks	
Parameter	Value
Total mass injected	5×10^{-16} kg
Escaped outlet	4.3×10^{-16} kg
Min time in the domain	3.9×10^{-1} sec
Max time in the domain	4.9 sec
Side by side heat sinks	
Parameter	Value
Total mass injected	5×10^{-16} kg
Escaped outlet	4.2×10^{-16} kg
Min time in the domain	4.1×10^{-1} sec
Max time in the domain	4.9 sec

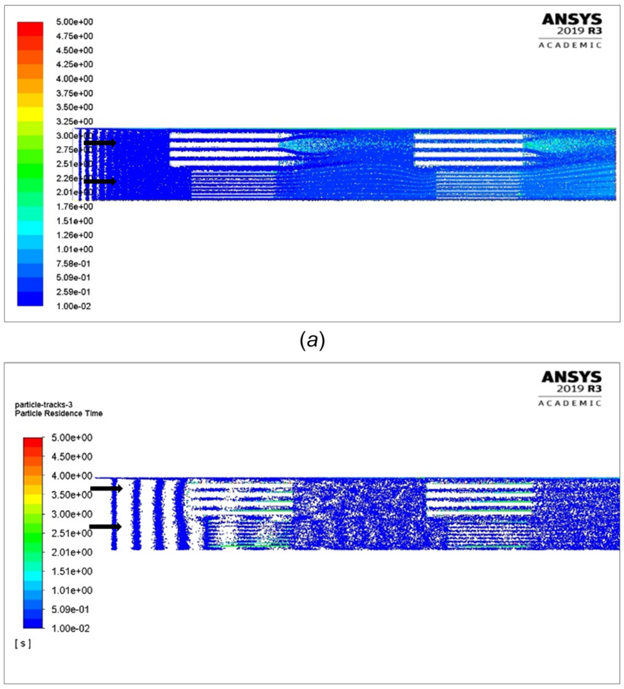

(*a*)

(*b*)

Fig. 7 Particle residence time in the flow domain for in-line heat sinks (*a*) low velocity and (*b*) high velocity

Table 4 Particle transfer summary for low and high-velocity particles

Low velocity	
Parameter	Value
Total mass injected	5×10^{-16} kg
Escaped outlet	4.2×10^{-16} kg
Min time in the domain	3.8×10^{-1}
Max time in the domain	4.5 sec
High velocity	
Total mass injected	5×10^{-16} kg
Escaped outlet	4.8×10^{-16} kg
Min time in the domain	1.4×10^{-1}
Max time in the domain	4.6 sec

set of DIMMs. The comparison of residence time and mass transfer through the outlet in both cases is shown in Table 4.

4.1.4 Effect of Heat Sink Cutouts. Cutouts can be provided on narrow as well as high form factor heat sinks to reduce system

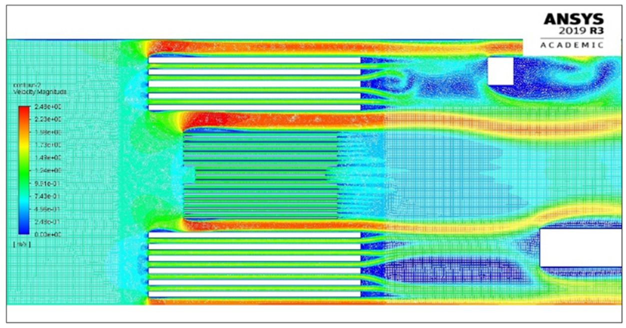

Fig. 8 Velocity profile of airflow inside the server with a center cutout in the heat-sink

Table 5 Particle summary for heat sink cutout case

With cutout	
Parameter	Value
Total mass injected	5×10^{-16} kg
Escaped outlet	4.2×10^{-16} kg
Min time in the domain	4.1×10^{-1} sec
Max time in the domain	4.9 sec
Without cutout	
Total mass injected	5×10^{-16} kg
Escaped outlet	4.4×10^{-16} kg
Min time in the domain	4.1×10^{-1} sec
Max time in the domain	4.98 sec

pressure drops. To observe the effect of change of geometry within the heat sink, a heat sink cutout was provided at the center of the sink as shown in Fig. 8. As can be seen in Table 5, the heat sink cutout caused a reduction in total mass escaping the outlet meaning more particles are trapped within the flow domain. Although the total reduction might seem a very small number, this can be significantly higher over hours of operation. This increase in particle count within the flow domain might be due to a reduction in total static pressure value around the fins which might cause a local deposition of particles in the surrounding region. This was also observed in particle residence time plots.

4.2 Results for Three-Dimensional Simulations. To comprehend the error in values obtained using 2D geometries for simplification instead of 3D geometries, the percentage variation in velocity and a visual comparison of the particle flow pattern were carried out. Figure 9 shows the velocity contours of 2D and 3D models of a server same geometric parameters. It can be seen that the airflow patterns in both cases are near similar, which is important from a particle dispersion point of view. The maximum velocity magnitude in the 2D case was 2.47 m/s and 1.69 m/s for the 3D model case. This means that the 2D simulations show approximately a 30% increase value of velocity values. Observing the particle tracks in Fig. 10, it was seen that the regions of maximum particle concentration were found in the trailing region behind both the heat sinks for both 2D and 3D modeling cases. This implies that while the simplification of using 2D models might not be accurate, it can aid in visualizing particle tracks with reduced computation time and resources.

Figure 11 shows the impact of server flow hood on particle dispersion within the server. Flow hoods and baffles are used in servers to force the airflow through the heat sinks for maximum heat transfer and reduce the thermal shadowing effect between two heat sinks place inline. It was seen from simulations that in presence of flow hood the particle-laden airflow disperses more as the

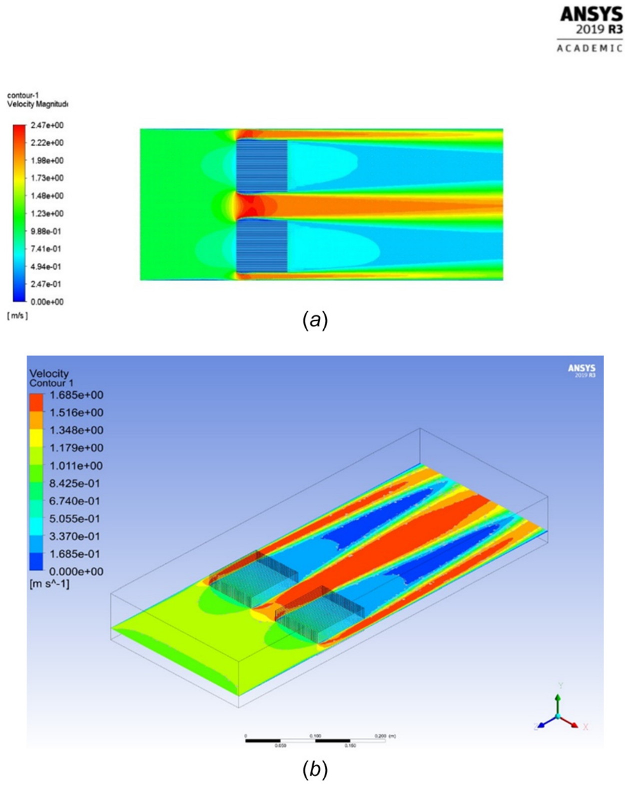

Fig. 9 Comparison of velocity magnitude values obtained from (*a*) 2D and (*b*) 3D simulations

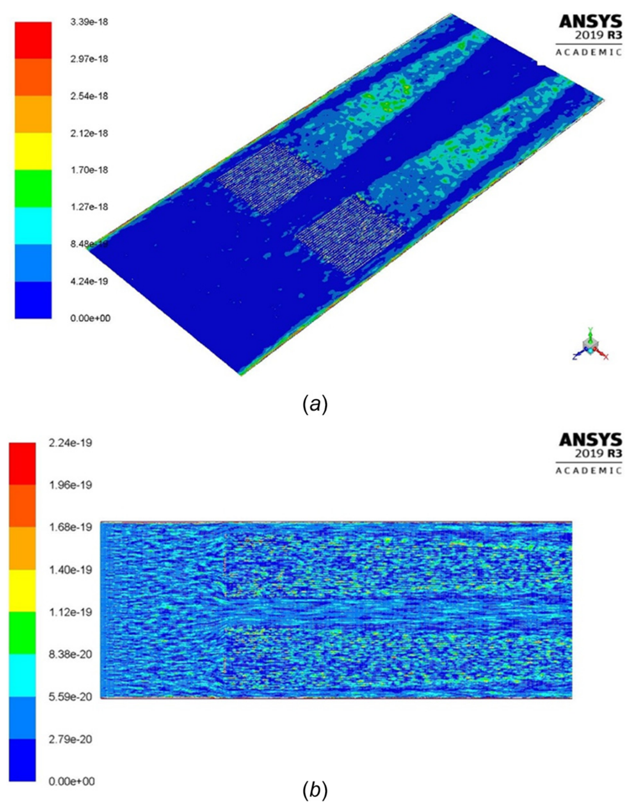

Fig. 10 Comparison of the particle flow path for (*a*) 3D simulation and (*b*) 2D simulation case

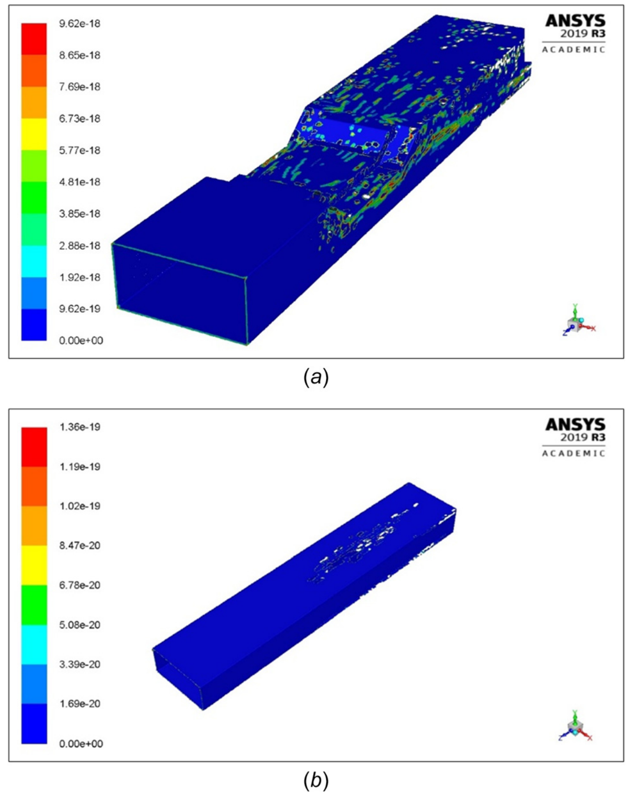

Fig. 11 Results for particle concentration inside the server with and without flow hood

Fig. 12 Figure 11: A comparison of dust deposition on the server chassis cover in (left) a clean laboratory data center (middle and right) in a modular data center located in polluted geography using an indirect/direct airside economization unit

flow cannot pass through the path of least resistance. This leads to higher particle concentration around the flow hood walls and chassis frame around the flow hood. These findings are consistent with a previous experimental investigation done by Shah et al. as shown in Fig. 12 [22].

As explained in Sec. 4.1.1, a tradeoff exists between using a curved edge heat sink which offers lower pressure drop and lower particle accumulation within the system. However, the thermal benefit of heat sinks with curved edges reduces due to a reduction of the total surface area of the fins, reducing its transfer capabilities as shown in Fig. 13. To reduce particle concentration within the ITE room, similar tradeoffs should be quantified for the type

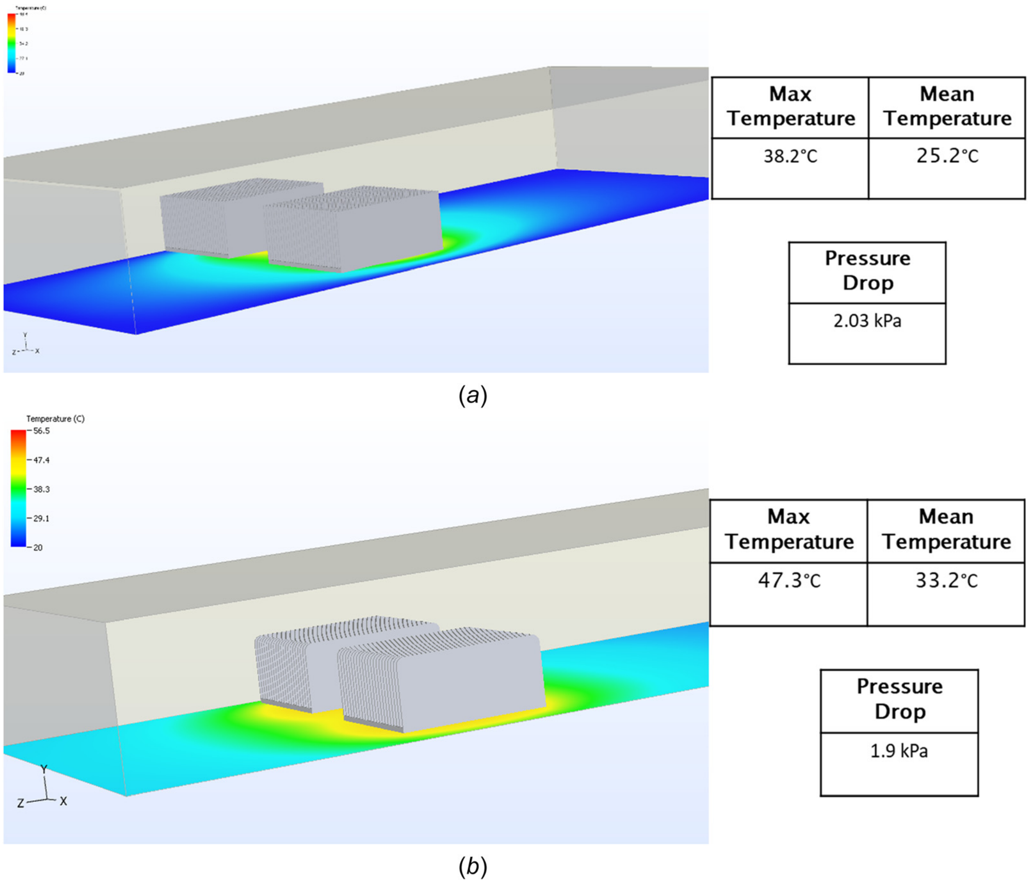

Fig. 13 Temperature contours showing thermal performance of (*a*) traditional heat sink and (*b*) heat sink with curved edges for pressure drop reduction

or rating of the MERV filter to be used. Higher arresting efficiency MERV filters will lead to a higher pressure drop or power consumption penalty but can also enhance the equipment's reliability. This should be done by correlating the typical annual particle concentrations. Data centers in the coastal regions may experience higher sea salt concentrations. Therefore, air filtration strategies should be implemented based on a thorough knowledge of outdoor air quality in terms of both the size and chemical composition of particles.

4.3 Results for Room Level Particle Flow. For room-level simulations, a CFD model of a current research modular data center was used as a simulation case. This modular unit uses a direct/indirect airside economizer for cooling. As seen in Fig. 14, a detailed model of the data center was first designed in 6SIGMA ROOM, a commercially available data center design software. Server pressure drop characteristics were used as input conditions for the ITE populated in the racks. An array of sensors was placed in the simulation case to monitor the pressure drop across the rack for the given inlet CFM to the ITE space inside the information technology (IT) pod. Based on this simulation, the pressure drop for the entire rack was obtained, which was then used as a criterion for determining the viscous and inertial resistance coefficients for the rack for a simplified CFD modeling case in ANSYS FLUENT.

As shown in Fig. 15, the first case for room level simulations was carried out with a rack as sold obstruction with a hot aisle partition. Using a similar CFD model setup as in ITE simulations in Sec. 3, the simulation results showed that the particles entering from the IT pod inlet, recirculate and stagnate primarily around the rack frames. The transient simulation results, as shown in Fig. 16 that the entire particle mass entering moves along with the airflow and moves toward the farther end of the pod. After striking this end, the particle mass circulates and reaches the bottom of the rack frames, rather than moving toward the outlet/hot-aisle side. A summary of particle flow data at room level is presented in Table 6.

5 Conclusions

This research presented a methodology for the assessment of particulate flow inside data center hardware and at room-level using simplified CFD models. Predictions for particle accumulation were made based on analysis of total elapsed time that the particles spend before escaping from the flow domain and by analyzing the difference of mass transferred between inlet and outlet of the flow domains. Based on the nature of flow obstructions present within the server, it was observed that while there might be little accumulation near thin features like DIMMs and heat sinks, the presence of other components and smaller features can significantly increase it. Also, features with aspect ratios of any dimension closer to 1 may have significant particle accumulation around them. On the contrary, features with larger lengths offer significantly less flow resistance and may be less vulnerable to deposition. Critical components, as per failure rates are concerned, are usually hard drives. Most of the storage servers today have separate hard drive bays. The servers where the hard drives are located toward the rear end might be more prone to exposure to particulates. It was also seen that higher velocities tend to increase accumulation on flat surfaces like fins and the DIMMs, therefore, for computational servers that are air-cooled, they might experience increased exposure to particles when the data center is operating in free air-cooling mode.

Further simplifications can be added to the modeling to reduce simulation time and resources. Based on accurate system pressure drop curves of real servers, multiphase simulations can be carried

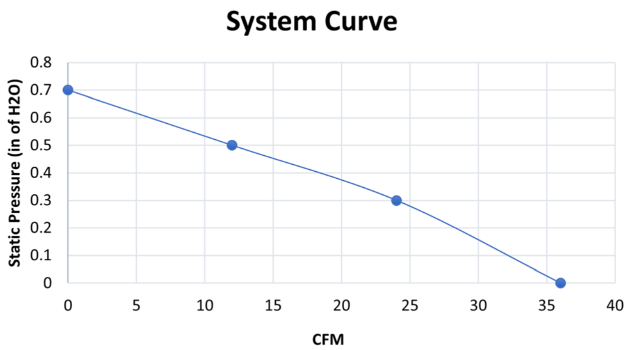

(*a*)

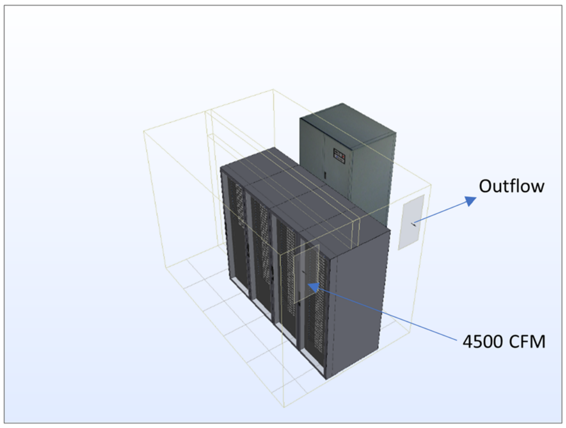

(*b*)

Fig. 14 (*a*) Plot for system curve used in 6SIGMAROOM for the servers and (*b*) isometric view of the modular data center used in the study

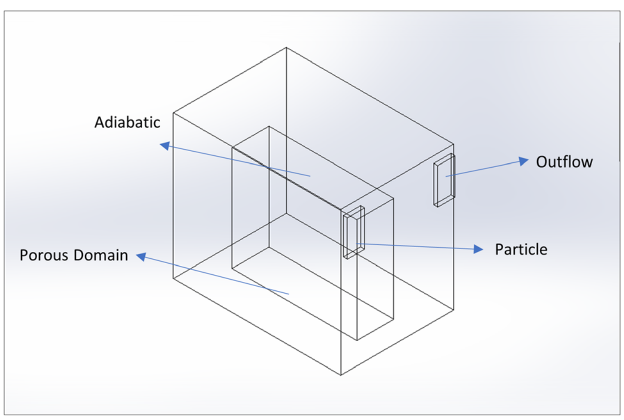

Fig. 15 An overview of the boundary conditions used for particle flow pattern analysis at room level

to represent the particle concentration distribution with the server as well as data center space. While there are methods and techniques to experimentally characterize the particulate contamination severity in the field environment [23,24], simple design and modeling-based CFD methods can be integrated with the data center heating, ventilation, and air-conditioning design process to ascertain the contaminant flow path in data centers using airside economization. This will help in identifying the locations inside the data center that can be critical in terms of contaminant concentrations and can help in mitigating the exposure of airborne contaminants to the ITE. Similar simulations for large-scale data centers need to be performed to formulate best practices for airside economized data centers.

Fig. 16 Distribution of particles inside the IT pod showing particle accumulation on top of the ITE rack

Table 6 Particle summary for room level simulation

Parameter	Value
Minimum elapsed time	5.776 sec
Total mass	2.8×10^{-15} kg
Escaped outlet	6.121×10^{-16} kg

Acknowledgment

This work is supported by NSF I/UCRC in Energy-Smart Electronic Systems (ES2). The authors would also like to extend special gratitude toward Mark Seymour and Kourosh Nemati of Future Facilities for their guidance and feedback throughout the project.

Funding Data

- NSF IUCRC (Award No. IIP-1738811; Funder ID: 10.13039/100000001).

Nomenclature

CFD = computational fluid dynamics
MERV = minimum efficiency reporting value
RANS = Reynolds averaged Navier–Stokes
Re = Reynolds number

References

[1] Niazmand, A., Chauhan, T., Saini, S., Shahi, P., Bansode, P. V., and Agonafer, D., 2020, "CFD Simulation of Two-Phase Immersion Cooling Using FC-72 Dielectric Fluid," ASME Paper No. IPACK2020-2595.
[2] Niazmand, A., Murthy, P., Saini, S., Shahi, P., Bansode, P., and Agonafer, D., 2020, "Numerical Analysis of Oil Immersion Cooling of a Server Using Mineral Oil and Al_2O_3 Nanofluid," ASME Paper No. IPACK2020-2662.
[3] Shah, J. M., Rizvi, S. H. I., Kota, I. S., Nagilla, S. R., Thakkar, D., and Agonafer, D., 2016, "Design Considerations Relating to Non-Thermal Aspects of Oil Immersion Cooling," ASME Paper No. IMECE2016-67320.
[4] Shahi, P., Saini, S., Bansode, P., and Agonafer, D., 2021, "A Comparative Study of Energy Savings in a Liquid-Cooled Server by Dynamic Control of Coolant Flow Rate at Server Level," IEEE Trans. Compon., Packaging Manuf. Technol., **11**(4), pp. 616–624.
[5] Shahi, P., Deshmukh, A., Hurnekar, H., Saini, S., Bansode, P. V., Kasukurthy, R., and Agonafer, D., 2021, "Design, Development, and Characterization of a Flow Control Device for Dynamic Cooling of Liquid-Cooled Servers," ASME J. Electron. Packag., **144**(4), p. 041008.
[6] ASHRAE Datacom Series, 2015, *Thermal Guidelines for Data Processing Environments*, 3rd ed., ASHRAE, Atlanta, GA.

[7] Open Compute Project, 2013, "Cooling an OCP Data Center in a Hot and Humid Climate," Open Compute Project, U.S., accessed Jan. 20, 2021, https://www.opencompute.org/blog/cooling-an-ocp-data-center-in-a-hot-and-humid-climate
[8] Google, 2022, "Efficiency," Google, Mountain View, CA, accessed Jan. 5, 2022, https://www.google. com/about/datacenters/efficiency/
[9] Johnstone, C., 2011, "Microsoft Shares Video Tour of its Cloud Datacenters," accessed Jan. 5, 2022, https://blog.insideo365.com/2011/07/microsoft-shares-video-tour-of-its-cloud-datacenters/
[10] ASHRAE Technical Committee 9.9., 2011, "Particulate and Gaseous Contamination Guidelines for Data Centers," ASHRAE Inc., Atlanta, GA.
[11] Shah, J. M., Anand, R., Saini, S., Cyriac, R., Agonafer, D., Singh, P., and Kaler, M., "Development of a Technique to Measure Deliquescent Relative Humidity of Particulate Contaminants and Determination of the Operating Relative Humidity of a Data Center," ASME Paper No. IPACK2019-6601.
[12] Thirunavakkarasu, G., Saini, S., Shah, J. M., and Agonafer, D., 2018, "Air Flow Pattern and Path Flow Simulation of Airborne Particulate Contaminants in a High-Density Data Center Utilizing Airside Economization," ASME Paper No. IPACK2018-8436.
[13] Seymour, M. J. A. A. M. A., and Jiang, J., 2000, "CFD Based Airflow Modelling to Investigate the Effectiveness of Control Methods Intended to Prevent the Transmission of Airborne Organisms," Air Distribution in Rooms (ROOMVENT 2000), Reading, UK, July 9–12, pp. 77–82.
[14] Jones, P. J., and Whittle, G. E., 1992, "Computational Fluid Dynamics for Building Air Flow Prediction- Current Status and Capabilities," Build. Environ., **27**(3), pp. 321–338.
[15] Chen, Q., and Zhang, Z., 2005, "Prediction of Particle Transport in Enclosed Environment," China Particuology, **3**(6), pp. 364–372.
[16] Saini, S., Shahi, P., Bansode, P., Siddarth, A., and Agonafer, D., 2020, "CFD Investigation of Dispersion of Airborne Particulate Contaminants in a Raised Floor Data Center," 36th Semiconductor Thermal Measurement, Modeling & Management Symposium (SEMI-THERM), San Jose, CA, Mar. 16–20, pp. 39–47.
[17] ANSYS, 2019, *ANSYS FLUENT Theory Guide, Chapter 16, Release 2019 R3*, ANSYS, Canonsburg, PA.
[18] ANSYS, 2019, *ANSYS FLUENT User's Guide, Chapter 24, Release 2019 R3*, ANSYS, Canonsburg, PA.
[19] Ibrahim, M., Shrivastava, S., Sammakia, B., and Ghose, K., 2012, "Thermal Mass Characterization of a Server at Different Fan Speeds," 13th InterSociety Conference on Thermal and Thermomechanical Phenomena in Electronic Systems, San Diego, CA, May 30–June 1, pp. 457–465.
[20] Lu, H., and Wang, Y., 2019, "Particle Deposition in Ventilation Ducts: A Review," Build. Simul., **12**(5), pp. 723–734.
[21] Frankenthal, R. P., Siconolfi, D. J., and Sinclair, J. D., 1993, "Accelerated Life Testing of Electronic Devices by Atmospheric Particles: Why and How," J. Electrochem. Soc., **140**(11), pp. 3129–3134.
[22] Shah, J. M., Awe, O., Gebrehiwot, B., Agonafer, D., Singh, P., Kannan, N., and Kaler, M., 2017, "Qualitative Study of Cumulative Corrosion Damage of Information Technology Equipment in a Data Center Utilizing Air-Side Economizer Operating in Recommended and Expanded ASHRAE Envelope," ASME. J. Electron. Packag., **139**(2), p. 020903.
[23] Shah, J. M., Anand, R., Singh, P., Saini, S., Cyriac, R., Agonafer, D., and Kaler, M., 2020, "Development of a Precise and Cost-Effective Technique to Measure Deliquescent Relative Humidity of Particulate Contaminants and Determination of the Operating Relative Humidity of a Data Center Utilizing Airside Economization," ASME. J. Electron. Packag,. **142**(4), p. 041103.
[24] Saini, S., Shah, J. M., Shahi, P., Bansode, P., Agonafer, D., Singh, P., Schmidt, R., and Kaler, M., 2021, "Effects of Gaseous and Particulate Contaminants on Information Technology Equipment Reliability—A Review," ASME. J. Electron. Packag., **144**(3), p. 030801.